Enhancing thermoelectric output power *via* radiative cooling with nanoporous alumina

Zhibing Zhan[a], Mohamed ElKabbash[a], Zihao Li[a], Xiaoyun Li[a], Jihua Zhang[a], James Rutledge[a], Subhash Singh[a,b], Chunlei Guo [a,b,]*

[a] The Institute of Optics, University of Rochester, Rochester, New York 14627, USA

[b] Changchun Institute of Optics, Fine Mechanics, and Physics, Changchun 130033, China

E-mail: guo@optics.rochester.edu

Keywords: thermoelectric generators, radiative cooling, nanoporous alumina, emissivity

Abstract: In this work, we demonstrate an enhanced thermoelectric output power using nanoporous alumina grown on aluminum (Al) surfaces. The improved power is due to enhanced thermal emissivity and passive radiative cooling associated with nanoporous alumina. We show that a careful balance between conduction, convection, and radiation heat transfer processes leads to optimal passive cooling for 30-40 μm thick alumina layers, while the nanopore size has a negligible effect. By growing a conformal alumina layer on an Al heatsink surface, the output power of a commercial thermoelectric generator (TEG) showed about 55% to 70% increase for temperature range of $150-250$ ℃ compared to using an untreated Al heatsink. With minimal footprint and no additional energy input, our passive cooling optimization method is a simple and facile way to enhance the TEG output power and can be extended to other applications that utilize Al heatsinks, *e.g.,* computers, cell-phones, and refrigerators.

Graphical Abstract

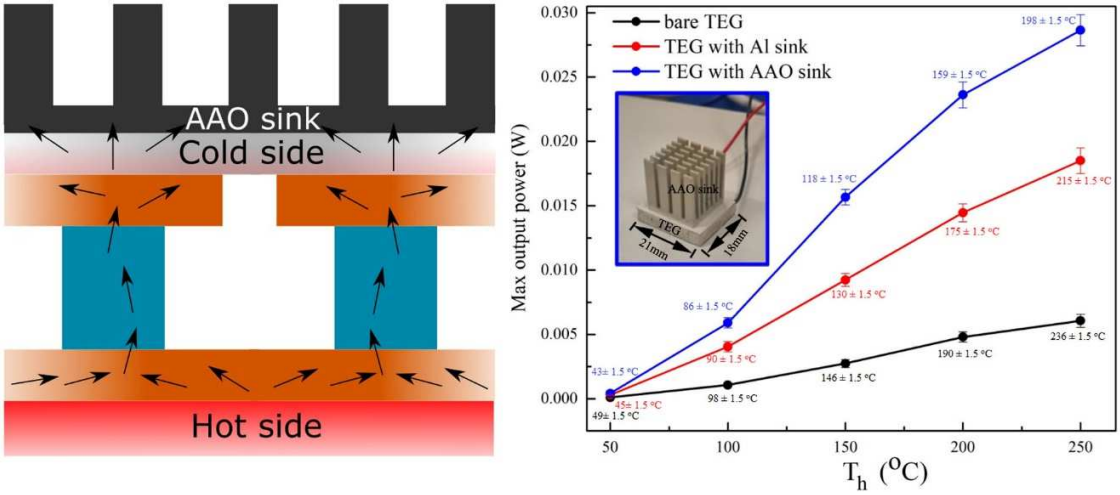

Research Highlights

- A method to enhance TEG output power is reported by using nanoporous alumina.
- The enhanced output power is due to passive radiative cooling.
- We determine the optimal thickness of alumina for radiative cooling.
- Using an alumina heatsink, we achieve ~ 55% - 70% increase in TEG output power.

1. Introduction

Thermoelectric generators (TEGs) convert heat flux (temperature gradient) into electricity directly *via* the Seebeck effect [1-4]. They have a wide range of applications including solar energy conversion [2], industrial and vehicle waste-heat recovery [5], geothermal energy harnessing [6], microelectronics, sensors and wearable devices powering [7]. TEG directly converts energy with no moving parts, which requires low maintenance, has long life span, and produces no noise [1, 2, 8, 9]. However, the low efficiency of TEGs prevent them from reaching their full potential. The TEG efficiency η_{TE} is given by:

$$\eta_{TE} = \frac{\Delta T}{T_h} \frac{\sqrt{1+(ZT)_M}-1}{\sqrt{1+(ZT)_M}+T_c/T_h} \quad (1)$$

which depends mainly on the temperature difference ΔT between the cold side temperature T_c and hot side temperature T_h of the generator, and on the generator's figure of merit $(ZT)_M$ [3, 10]. Many works focused on finding materials with higher figure of merit at different temperature range [4]. Furthermore, recent works have optimized the design of the hot side heat exchanger in the context of solar thermoelectric generation by designing selective light absorbers with low emissivity in the blackbody radiation band [3, 10]. On the other hand, little attention is given to the practical limitations on the cold side of the heat exchangers with the assumption that T_c can be minimized down to room temperature *via* heat spreading and convective cooling [10]. However, this approach ignores the space limitation in many applications that can render thermoelectric generation inefficient. Other active cooling techniques using a fan or water to cool down thermoelectric modules require a substantial amount of energy and resources to carry heat away, which reduce the overall system efficiency dramatically, and have narrow potential particularly for applications of limited scale [3, 11].

On the other hand, the field of thermal photonics has flourished, reviving old interest in radiative cooling for more extreme applications, *e.g.,* daytime radiative cooling and sub-freezing radiative cooling [12-17]. Passive radiative cooling dissipates heat by thermal radiation [18, 19]. Since radiative cooling is a surface property, proper surface functionalization can enhance radiative cooling without additional energy consumption or footprint [18, 19]. In the context of energy applications, radiative cooling was theoretically proposed to increase photovoltaic solar cell efficiency by decreasing the solar cell temperature as much as 18.3 ℃ below ambient [20], and a 13 ℃ cooling was demonstrated experimentally [21]. In addition, radiative cooling of thermophotovoltaics modules is estimated to possibly lead to 18% increase in efficiency [22]. Very recently, radiative cooling of TEG was used to instigate a temperature difference, with respect to room temperature, hence, power generation by lowering the cold side temperature below ambient temperature [19]. Accordingly, utilizing radiative cooling to improve other energy applications that rely on proper thermal management is highly relevant. However, a systematic study on optimizing TEG thermal management to increase its efficiency *via* radiative cooling has not been performed.

In this work, we produce nanopatterned alumina and systematically study the heat exchange properties of alumina layers grown on an aluminum (Al) surfaces to maximize the output power of TEGs. The alumina layers we designed exhibit strong spectral emissivity within the blackbody radiation band of TEGs. We show that the spectral emissivity depends strongly on its thickness and weakly on the nanopores size. The optimal thickness of alumina layer for enhancing TEG output power relies on balancing the template's convection, conduction, and radiation heat exchange properties and does not simply scale with emissivity. By growing a conformal alumina layer on a commercial Al heatsink, we obtain a output power increase as high

as 70% compared to using an untreated Al heatsink. Our work shows that radiative cooling can be an integral thermal management technique and can significantly improve the performance of TEGs for wide range of applications.

2. Experimental section

Commercial Bi-Te based TEGs (module of TE-MOD-1W2V-21S) with size of 18 mm × 21 mm were purchased from TEGpro^{tm}. Bi-Te based TEG power modules can operate at temperatures as high as 230 °C continuously. Polished Al foils with the thickness of 0.2 mm and purity >99% were purchased from GoodFellow. Al heatsinks with the size of 15 mm ×15 mm ×15 mm were purchase from Digi-Key. Every Al heatsink has 28 fins (4×7). Acetone (99.5%), Copper (II) chloride (98%), chromium (VI) oxide (99%), phosphoric acid (85%), and oxalic acid (98%) used for preparation and characterization of the samples were purchased from Alfa Aesar.

Al foils were cut to discs with diameter of 23 mm, then they were degreased and washed by acetone and DI water in an ultrasound cleaner. Al foil was first anodized in 0.3M oxalic acid solution at 15 °C for 5 h at 40 V. The first alumina layer was removed in a mixture solution of H_3PO_4 (6 wt%) and H_2CrO_4 (1.8 wt%) at 60 °C for 8 h leaving an Al foil ~ 160 μm thick. The second time anodization is carried out under the same condition as that of the first one. The duration of the second anodization determines the thicknesses of alumina layers, which are about 1.25, 2.5, 3.75, 5.0, 6.25, 7.5 and 12.5 h for AAO layers with thicknesses of 10, 20, 30, 40, 50, 60, and 100 μm, respectively. For the anodization of Al heatsink, its flat side was first cleaned and connected to a copper wire and then sealed by a layer of insulator epoxy (B-J weld company). After that, the anodization of Al heatsink was carried out the same as that of the Al foil. To widen the size of nanopores in alumina layer, samples were etched by H_3PO_4 solution (5 wt%) at 40 °C for 15, 30, and 45 min.

TEG measurement are performed on a hotplate with maximum temperature of 350 °C. Al foils and heatsinks were mounted on the cold side of a TEG by a high temperature conductive paste (Omega^{TM}). The hot side of the TEG was connected to the hotplate by the same paste. After the sample is connected and the hotplate preset temperature (50, 100, 150, 200, and 250 °C) is stable for at least 5 min, TEG output measurement were taken. Tempratures and IR images are measured and took by an IR thermometer (FLIR TG 167). The output current and voltage of the TEG were recorded by a source meter (Keithley 2400), and the output power was calculated based on the measured current and voltage. Every measurement was repeated for at least five times. The measurement environment always kept at 21°C.

The surface structures of Al foil and alumina layers were characterized by Scanning Electron Microscopy (SEM). The SEM is a Zeiss- Auriga Field Emission SEM operating at an accelerating voltage of 5 kV. Emissivity of the samples was measured using Fourier transform infrared (FT-IR) spectroscopy (Nicolet 6700 FT-IR spectroscopy, Thermo Scientific, USA), where the measured range of the wavelength was 2.5–16 μm.

3. Results and discussions

For a conventional TEG, as shown in Figure 1a, the temperature difference between the hot and cold sides of the TEG diminishes due to the thermal conductivity of the thermoelectric module. Adding an Al plate on the cold side of the TEG may be ideal for convective cooling due to the high thermal conductivity of Al. However, Al has negligible emissivity in the IR where the blackbody radiation band of most TEG resides, *i.e.*, the only cooling mechanism is convective cooling *via* natural convection or forced convection [11]. Increasing the area A of the Al heatsink would increase the overall cooling power $\dot{Q}$ given by

$$\dot{Q} = A\,q;\; q = \bar{\varepsilon}\sigma\,(T_c^4 - T_{amb}^4) + U\,(T_c - T_{amb}) \qquad (2)$$

where q is the heat flux from the TEG cold side, which is determined by radiative, convective and conductive cooling, $\bar{\varepsilon}$ is the emissivity, σ is Stefan-Boltzmann constant, U is the overall heat transfer coefficient of the TEG cold side, and T_{amb} is the ambient temperature [23]. However, increasing the heatsink area may not be suitable for many applications and is less cost effective. On the other hand, the cooling power of an Al heatsink can be increased by increasing the net heat flux. In particular, nanoporous anodic aluminum oxide (AAO) templates enjoy high $\bar{\varepsilon}$ in the IR due to strong phonon-polariton excitations and high surface roughness which lead to strong radiative cooling (Figure 1b) [24]. Although its thermal conductivity is low, thin AAO templates are sufficient to realize strong absorptivity and convective cooling will not be significantly jeopardized as we will show.

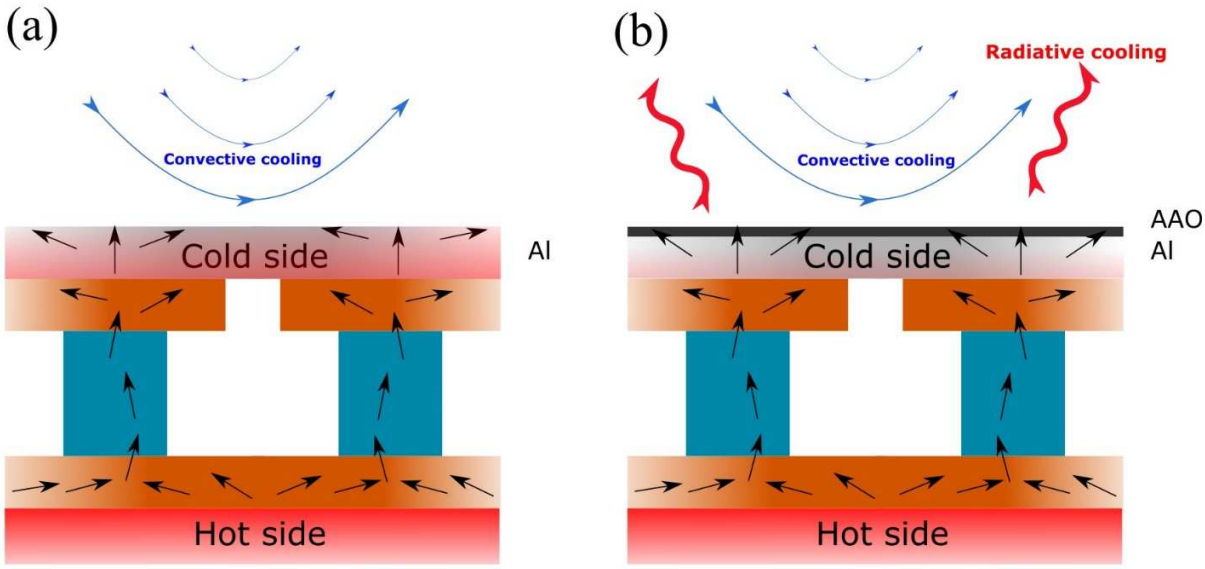

Figure 1. Radiative cooling of TEG with AAO. (a) A TEG has a receiver of thermal energy on its hot side that is thermally connected to the thermoelectric module. The module is in turn thermally connected to the cooling system. Using Al only, cooling by natural or forced convection is possible. (b) By anodizing the Al, the AAO template enable strong radiative

cooling while maintaining convective cooling. Cooling is necessary to maintain sufficient temperature difference across the module.

Figure 2a shows an SEM image of a polished Al surface. After anodization, Al surface produces overall uniform nanohole array over the entire treated surface as shown in Figure 2b. A SEM image showing the large area AAO can be found in Figure S1. The AAO template takes the form of a close-packed array of hexagonal cells, each containing a cylindrical central hole orthogonal to the Al surface [25, 26]. The SEM image of the AAO cross-section and underlying Al substrate are shown in Figure 2c to 2e. Most AAO holes are comprised of a single channel, which extends from the surface down to an alumina barrier layer between the bottom of the channel and the Al substrate. This thin non-porous barrier layer has a hemispherical and scalloped geometry, as shown in Figure 2e. The pore diameter and cell size of the AAO shown here are approximately 30 and 100 nm, respectively, which are the stranded parameters for AAO template fabricated in oxalic acid solution using anodic voltage of 40 V [27-29]. The thickness of the AAO layer is determined by the anodization time with estimated growth rate of ~ 8 μm/h in our experimental conditions. More SEM images of AAOs with different thicknesses are shown in the supplementary information Figure S2 and S3.

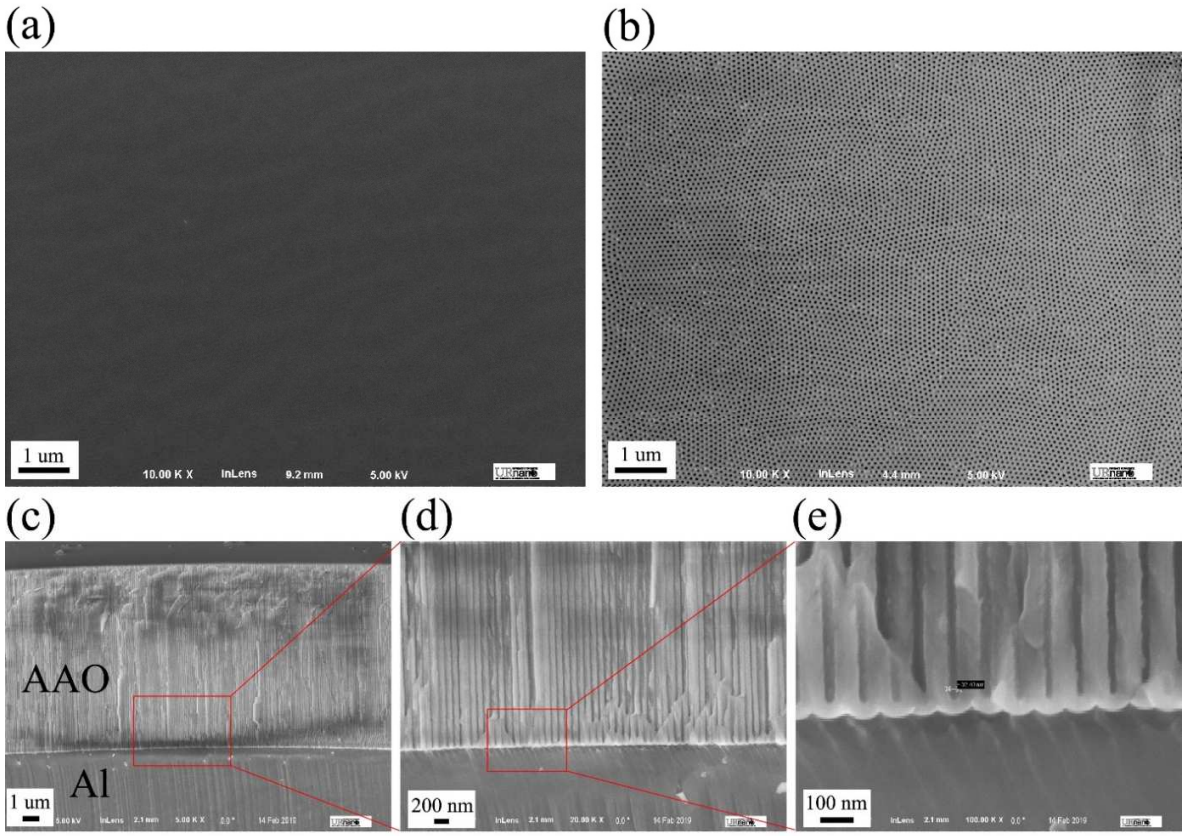

Figure 2. Characterization of AAO templates. Top-view SEM images of a polished Al surface (a) and AAO surface (b). Cross-section SEM images of the AAO layer grown on the surface of an Al substrate at various magnifications (c to e).

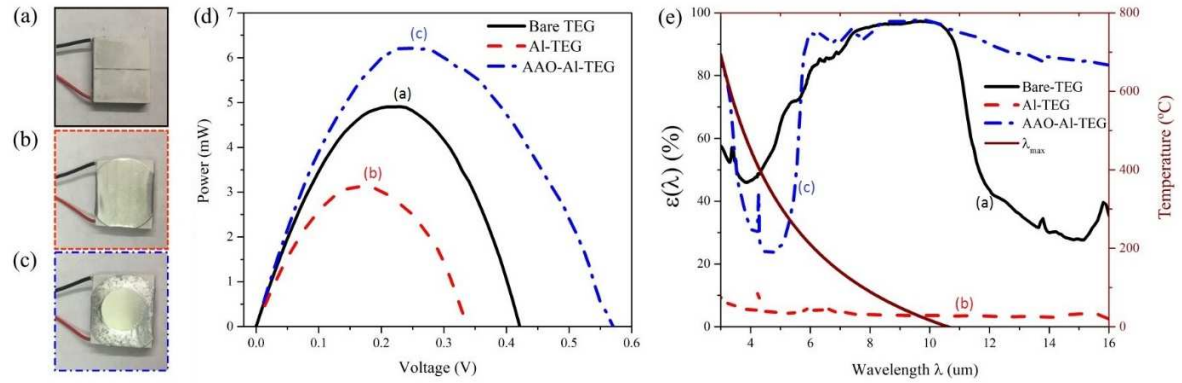

Figure 3. Thermoelectric generation with flat cold side surface. Without adding a heatsink we compare the TEG performance of three systems (a) a bare TEG with a cold side surface made of ceramics (Bare-TEG), (b) a TEG with an Al foil attached to its back (Al-TEG), and (c) a TEG with AAO template grown on Al foil attached to its back (AAO-Al-TEG). (d) The measured output TEG power *vs.* voltage for the systems of the Bare-TEG, Al-TEG and AAO-Al-TEG. (e) The measured spectral emissivity for the three systems and the peak blackbody radiation wavelength λ_{max}.

To demonstrate the importance of AAO radiative cooling, we compare the TEG output powers for bare TEG where the cold side of TEG is made of ceramic material (Bare-TEG, see Figure 3a), TEG with an Al foil attached to its cold side (Al-TEG, see Figure 3b), and a TEG with anodized Al attached to its cold side (AAO-Al-TEG, see Figure 3c). Figure 3d shows the output TEG power *vs.* voltage when the hot side keeps temperature at 200 ℃ for the three systems. Figure S4 shows how to determine the TEG output power from the measured I-V characteristics. Interestingly, Al-TEG shows lower output power compared to Bare-TEG, while AAO-Al-TEG has the highest output power. The AAO-Al-TEG system exhibit maximum output power enhancement by ~ 30% and 100% compared to the Bare-TEG and Al-TEG systems,

respectively (Figure 3d). Furthermore, the measured tempratures of the Al-TEG and AAO-Al-TEG systems by an IR thermometer confirmed that AAO structures have lower surface temperature (Supporting Information, Figure S5).

Figure 3e shows the measured spectral emissivity $\varepsilon(\lambda)$ of the cold side for the three systems using Fourier transform infrared (FT-IR) spectroscopy which measures the angular absorptance (a typical spectrum in UV-Vis-NIR range is shown in Figure S6). The measured spectral emissivity is considered equivalent to spectral absorptance since AAO is treated as reciprocal material with symmetric permittivity and permeability tensors, thus satisfying Kirchhoff's law of radiation [12]. Al-TEG has the lowest spectral emissivity over the entire IR spectrum, thus, least radiative cooling power, as expected. The bare TEG, surprisingly, has strong spectral emissivity over a wide range of wavelengths. For the majority of wavelengths, however, AAO-Al-TEG system has the highest spectral emissivity. Using Wien displacement law [23], we can calculate the peak blackbody radiation wavelength λ_{max} for different temperatures $T = 2897.8/\lambda_{max}$, where λ is in microns. Clearly, for temperatures up-to ~225^{o}C, the spectral emissivity of AAO-Al-TEG is higher at the maximum blackbody radiation compared to Bare-TEG. In all cases, the ability to construct cheap heatsinks with large surface area and cooling power from Al makes the AAO an realistic option for hybrid cooling.

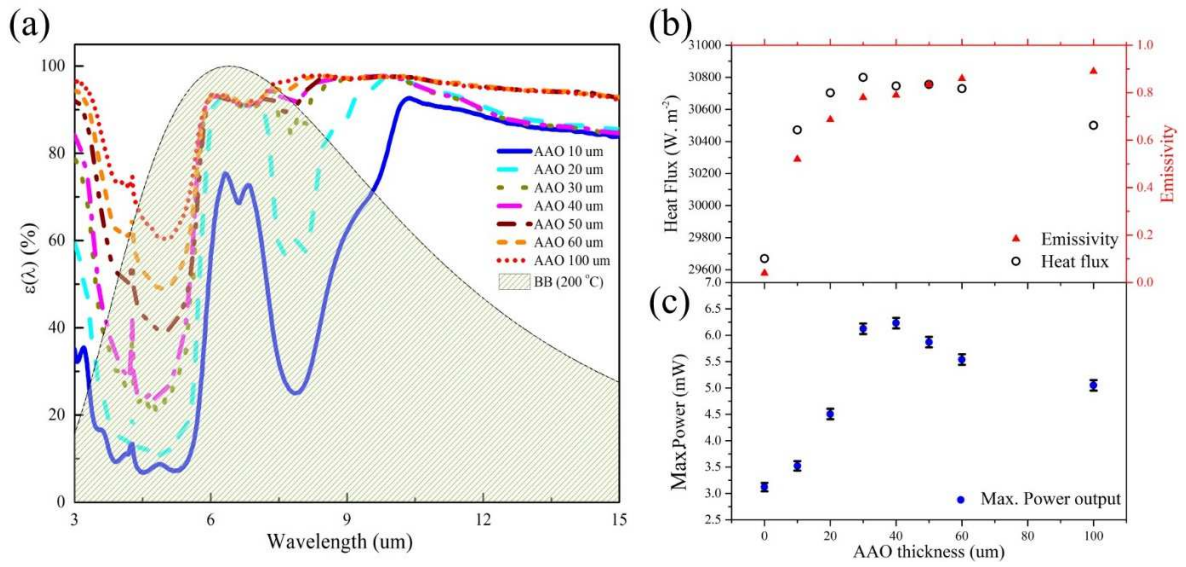

Figure 4. AAO spectral emissivity and TEG power as a function of AAO thicknesses ($\boldsymbol{t_{AAO}}$). (a) Spectral emissivity for different AAO thicknesses (10, 20, 30, 40, 50, 60, and 100 μm), and the blackbody radiation spectrum at 200 ℃. (b) The calculated emissivity $\bar{\varepsilon}$ for a blackbody radiating at 200 ℃ increases with increasing AAO thickness, however, the net heat flux is maximum at $t_{AAO} \sim 30 - 40\ um$. (c) The measured maximum output TEG power as a function of t_{AAO} follows a similar trend to the heat flux.

Figure 4a shows $\varepsilon(\lambda)$ for AAO templates with various thicknesses grown on Al substrates and the blackbody radiation spectrum at 200 ℃. Clearly, as the AAO thickness increases from 10 μm to 100 μm, $\varepsilon(\lambda)$ increases over the entire measured IR spectrum. The emissivity $\bar{\varepsilon}$ for the different systems, shown in Figure 4b, is given by

$$\bar{\varepsilon} = \frac{\int_0^\infty d\lambda\, \varepsilon(\lambda)/\{\lambda^5[exp(hc/\lambda kT) - 1]\}}{\int_0^\infty d\lambda/\{\lambda^5[exp(hc/\lambda kT) - 1]\}} \quad (3)$$

where h is Plank's constant, c is the speed of light, λ is the wavelength, k is Boltzmann constant [23]. The measured temperatures of different surfaces by an IR thermometer are shown in

supporting inforamtion Table S1. However, in order to calculate the heat flux from the TEG cold side, we need to also consider the effect of the AAO thickness on the convective cooling process. The overall heat transfer coefficient U in equation 2 is given by

$$U = \left[\frac{t_{Al}}{k_{Al}} + \frac{t_{AAO}}{k_{AAO}} + \frac{1}{h_{air}}\right]^{-1} \quad (4)$$

where t_{Al} and t_{AAO} are the thicknesses of Al and AAO, respectively, and $k_{Al} = 273\ W\ m^{-1}K^{-1}$, and $k_{AAO} \sim 0.8\ W\ m^{-1}K^{-1}$ are the thermal conductivity of Al, and AAO respectively, and h_{air} is the heat transfer coefficients of air which is ~ 200 $W\ m^{-2}K^{-1}$ in a lab room with operating hvac system [23, 30]. Consequently, thicker AAO reduces U, and thinner Al increases U. Although the anodization process leads to simultaneous increase in AAO thickness and decrease in Al thickness, changes in t_{Al} has negligible effect on U due to the high k_{Al}value. The calculated net heat flux for different AAO thicknesses, q (200 ℃), peaks at ~ 30-40 μm of AAO and does not simply increase with increasing the emissivity (Figure 4b). According to equation 1, the TEG efficiency is related to $(ZT)_M$, and proportional to the temperature difference $\Delta T = T_h - T_c$. In our case (bismuth telluride TEG using at around 200 ℃), reducing T_c leads to a slight increase in $(ZT)_M$ [4, 31, 32]. Therefore, by decreasing T_c, for a given T_h, we increase the TEG output power and efficiency. The output TEG power *vs.* voltage of AAO samples with various thicknesses are measured (Figure S7), and the maximum output power are shown in Figure 4c. As expected, maximum TEG output power as a function of AAO thickness follows a similar trend to the net heat flux with optimal performance at ~ 30-40 μm. We note that the optimal AAO thickness would depend on the TEG environment which could modify U due to changes in h_{air} or $\bar{\varepsilon}$ through changes in operation temperature. In our conditions, the increase in the temperature difference across the TEG, compared to the bare TEG case, leads to an increase in thermoelectric generation efficiency.

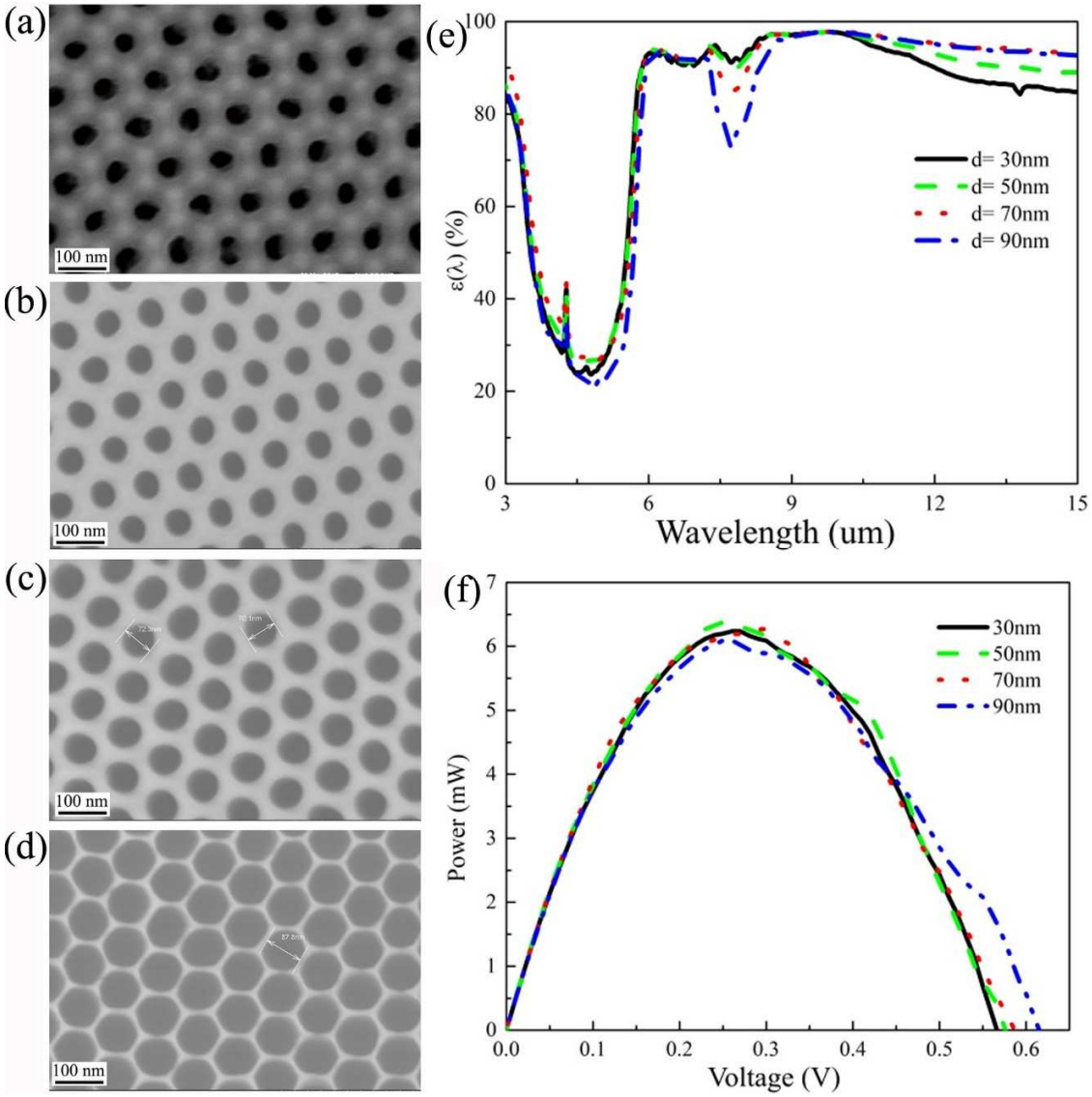

Figure 5. Top-view SEM images of AAO surfaces with nanohole diameters of about 30 nm (a), 50 nm (b), 70 nm (c) and 90 nm (d), and their corresponding spectral emissivity (e). (f) the measured TEG output powers *vs.* voltage for AAOs with diameters of ~30, 50, 70, 90 nm. The thickness of the AAO layer at here are about 40 μm.

To further optimize the system , we investigated the effect of the nanohole size on the radiative cooling properties of AAO. As an important parameter in AAO, the diameter of the AAO nanoholes can be widen by using H_3PO_4 solution [28, 33]. For comparison, we varied the

AAO pore size using H_3PO_4 solution (5 wt%) at 40 °C for a 40 μm thick AAO template. The as prepared AAO has a pore diameter of ~30 nm. Considering the period of AAO nanohole array is ~100 nm, the maximum pore diameter possible is ~90nm. Further etching will result in the decomposition of the nanohole arrays (see Supplementary Information, Figure S8). Top view SEM images of AAO templates with nanopore diameter d = 30 nm, 50 nm, 70 nm, and 90 nm are shown in Figure 5a, 5b, 5c, and 5d, respectively. The measured emissivity of all samples is presented in Figure 5e, showing weak dependence on the nanopore size with relatively lower emissivity for larger d. Consequently, the measured TEG output power is almost independent of the nanopore size (Figure 5f). We note that the thermal conductivity of AAO templates, k_{AAO}, depends on the porosity [30, 34]. However, the overall heat transfer coefficient dependence on k_{AAO} is scaled by the AAO thickness, *i.e.,* $\partial U/\partial k_{AAO} = t_{AAO}\left[k_{AAO}\left(\frac{t_{Al}}{k_{Al}}+\frac{1}{h_{air}}\right)+t_{AAO}\right]^{-2}$. Hence, for relatively thin AAO templates, the change in thermal conductivity has minor effect on the net heat flux. But for thicker AAO templates, the heat flux depends on the k_{AAO} (see Figure S9). To further confirm the prediction of our model, we compared the thermoelectric generation performance of a 100 μm AAO template with nanopore size of 30 nm and 70 nm. As shown in Figure S10, the system with higher porosity, *i.e.,* lower thermal conductivity, has lower TEG output power as predicted by our model.

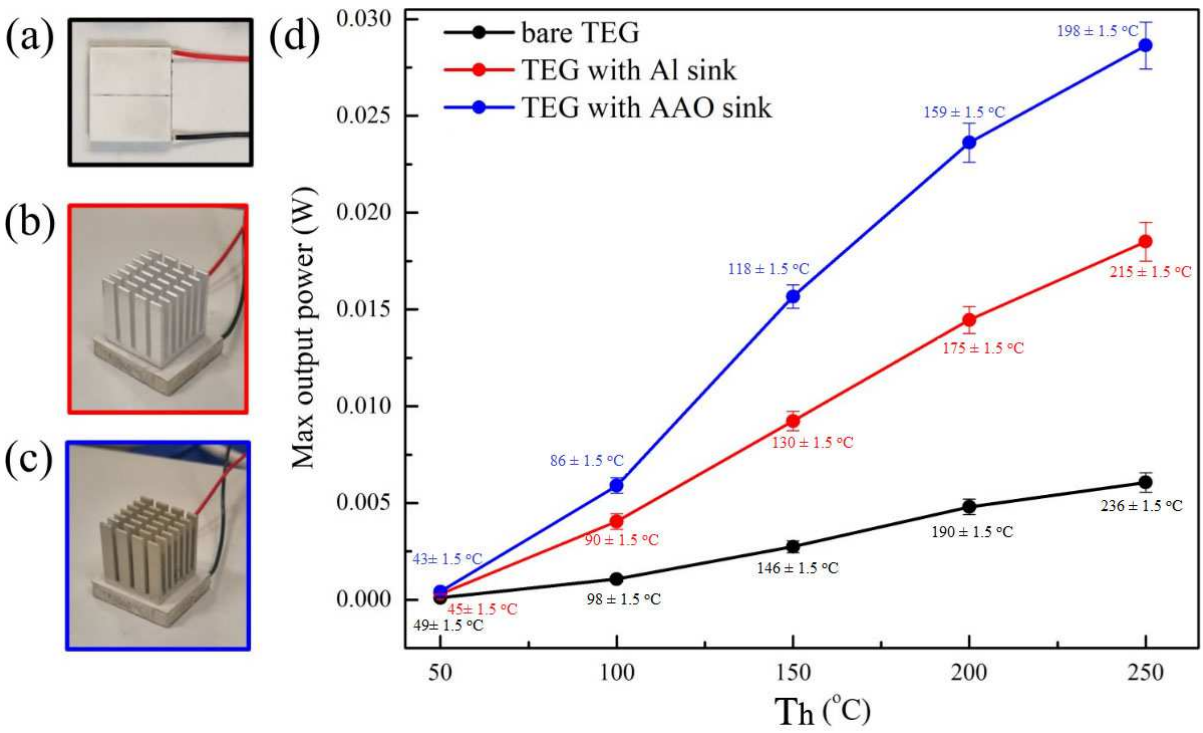

Figure 6. Boosting TEG output power using AAO template grown on Al heatsink: (a), (b) and (c) show photos of a bare TEG, a TEG with a commercial Al heatsink attached to its back, and a TEG with AAO conformally grown on the commercial Al heatsink (AAO sink). (d) The maximum output power of the TEG for the three systems as a function of hot side temperature (T_h) (The corresponding measured cold side temperatures, T_C, for the three systems at different T_h are labeled near each data point).

As we mentioned earlier, the benefit of AAO-Al system is that one can easily construct a cheap large-area heatsink from Al on which we can grow optimal AAO template to boost the heatsink cooling efficiency. We anodized a commercial Al heatsink growing ~ 40 μm AAO template and compared its performance with the as-purchased Al heatsink (see Supplementary information Figure S11). Photos of the bare TEG, TEG with Al sink, and TEG with AAO sink are shown in Figure 6a, 6b, and 6c, respectively. The maximum output power measured for the three systems as a function of hot-side temperature is shown in Figure 6d. The measured cold side

temperature T_C for the three systems at different T_h are shown near each data point. Clearly the TEG with AAO sink has better performance for all temperatures and the output power increases by ~ 55% to 70% for temperature range of $150 - 250$ ℃. This remarkable enhancement with minimal footprint highlights the significant role of radiative cooling based on AAO templates in energy and thermal management applications.

4. Conclusions

To conclude, we showed that the strong spectral emissivity of AAO templates conformally grown on Al surfaces can significantly increase the output power of TEGs. By optimizing the parameters of AAO templates, we can optimize the radiative, convective, and conductive cooling processes. Growing the optimal AAO template for cooling on a commercial Al heatsink increases its cooling efficiency. The TEG output power increased by ~ 55% to 70% when using anodized Al heatsink compared to the commercially obtained Al heatsink. Due to no requiring additional volume and energy to operate cooling units, our detailed study leads to a universal and cost-effective method to increase the cooling efficiency of heatsinks which are integral components in fridges, cellphones and computers, as well as other energy applications, e.g., cooling photovoltaic cells.

Acknowledgements
This work was supported by the Bill & Melinda Gates Foundation (OPP1119542), National Science Foundation (1701163 & 1722169), and the US Army Research Office (W911NF-15-1-0319) grants.

Appendix A. Supplementary material

Supplementary data associated with this article can be found in the online version at doi:10.1016/j.nanoen.

References

[1] D.M. Trucchi, A. Bellucci, M. Girolami, P. Calvani, E. Cappelli, S. Orlando, R. Polini, L. Silvestroni, D. Sciti, A. Kribus, Solar Thermionic-Thermoelectric Generator (ST(2)G): Concept, Materials Engineering, and Prototype Demonstration, Adv. Energy Mater., 8 (2018) 1802310.
[2] D. Champier, Thermoelectric generators: A review of applications, Energy Conv. Manag., 140 (2017) 167-181.
[3] D. Kraemer, Q. Jie, K. McEnaney, F. Cao, W.S. Liu, L.A. Weinstein, J. Loomis, Z.F. Ren, G. Chen, Concentrating solar thermoelectric generators with a peak efficiency of 7.4%, Nat. Energy, 1 (2016) 1-8.
[4] B. Poudel, Q. Hao, Y. Ma, Y.C. Lan, A. Minnich, B. Yu, X.A. Yan, D.Z. Wang, A. Muto, D. Vashaee, X.Y. Chen, J.M. Liu, M.S. Dresselhaus, G. Chen, Z.F. Ren, High-thermoelectric performance of nanostructured bismuth antimony telluride bulk alloys, Science, 320 (2008) 634-638.
[5] L.E. Bell, Cooling, heating, generating power, and recovering waste heat with thermoelectric systems, Science, 321 (2008) 1457-1461.
[6] L.P. Liu, Feasibility of large-scale power plants based on thermoelectric effects, New J. Phys., 16 (2014) 123019.
[7] Y.S. Jung, D.H. Jeong, S.B. Kang, F. Kim, M.H. Jeong, K.S. Lee, J.S. Son, J.M. Baik, J.S. Kim, K.J. Choi, Wearable solar thermoelectric generator driven by unprecedentedly high temperature difference, Nano Energy, 40 (2017) 663-672.
[8] P. Aranguren, D. Astrain, A. Rodriguez, A. Martinez, Experimental investigation of the applicability of a thermoelectric generator to recover waste heat from a combustion chamber, Appl. Energy, 152 (2015) 121-130.
[9] F. Hao, P.F. Qiu, Y.S. Tang, S.Q. Bai, T. Xing, H.S. Chu, Q.H. Zhang, P. Lu, T.S. Zhang, D.D. Ren, J.K. Chen, X. Shi, L.D. Chen, High efficiency Bi2Te3-based materials and devices for thermoelectric power generation between 100 and 300 degrees C, Energy Environ. Sci., 9 (2016) 3120-3127.
[10] D. Kraemer, B. Poudel, H.P. Feng, J.C. Caylor, B. Yu, X. Yan, Y. Ma, X.W. Wang, D.Z. Wang, A. Muto, K. McEnaney, M. Chiesa, Z.F. Ren, G. Chen, High-performance flat-panel solar thermoelectric generators with high thermal concentration, Nat. Mater., 10 (2011) 532-538.
[11] M. Sajid, I. Hassan, A. Rahman, An overview of cooling of thermoelectric devices, Renew. Sust. Energ. Rev., 78 (2017) 15-22.
[12] S.H. Fan, Thermal Photonics and Energy Applications, Joule, 1 (2017) 264-273.
[13] B. Bhatia, A. Leroy, Y.C. Shen, L. Zhao, M. Gianello, D.H. Li, T. Gu, J.J. Hu, M. Soljacic, E.N. Wang, Passive directional sub-ambient daytime radiative cooling, Nat. Commun., 9 (2018) 8.
[14] Z. Chen, L.X. Zhu, A. Raman, S.H. Fan, Radiative cooling to deep sub-freezing temperatures through a 24-h day-night cycle, Nat. Commun., 7 (2016) 5.
[15] J. Mandal, Y.K. Fu, A.C. Overvig, M.X. Jia, K.R. Sun, N.N. Shi, H. Zhou, X.H. Xiao, N.F. Yu, Y. Yang, Hierarchically porous polymer coatings for highly efficient passive daytime radiative cooling, Science, 362 (2018) 315-318.
[16] Y. Zhai, Y.G. Ma, S.N. David, D.L. Zhao, R.N. Lou, G. Tan, R.G. Yang, X.B. Yin, Scalable-manufactured randomized glass-polymer hybrid metamaterial for daytime radiative cooling, Science, 355 (2017) 1062–1066.

[17] A.W. Harrison, M.R. Walton, RADIATIVE COOLING OF TIO2 WHITE PAINT, Sol. Energy, 20 (1978) 185-188.
[18] J. Lee, D. Kim, C.H. Choi, W. Chung, Nanoporous anodic alumina oxide layer and its sealing for the enhancement of radiative heat dissipation of aluminum alloy, Nano Energy, 31 (2017) 504-513.
[19] E.Z. Mu, Z.H. Wu, Z.M. Wu, X. Chen, Y. Liu, X.C. Fu, Z.Y. Hu, A novel self-powering ultrathin TEG device based on micro/nano emitter for radiative cooling, Nano Energy, 55 (2019) 494-500.
[20] L.X. Zhu, A. Raman, K.X. Wang, M. Abou Anoma, S.H. Fan, Radiative cooling of solar cells, Optica, 1 (2014) 32-38.
[21] L.X. Zhu, A.P. Raman, S.H. Fan, Radiative cooling of solar absorbers using a visibly transparent photonic crystal thermal blackbody, Proc. Natl. Acad. Sci. U. S. A., 112 (2015) 12282-12287.
[22] Z.G. Zhou, X.S. Sun, P. Bermel, Radiative cooling for thermophotovoltaic systems, Proc. SPIE, 9973 (2016) 997308.
[23] Y.A. Çengel, Heat Transfer: A Practical Approach, (2003).
[24] Y. Fu, J. Yang, Y.S. Su, W. Du, Y.G. Ma, Daytime passive radiative cooler using porous alumina, Sol. Energy Mater. Sol. Cells, 191 (2019) 50-54.
[25] A. Al-Haddad, Z.B. Zhan, C.L. Wang, S. Tarish, R. Vellacheria, Y. Lei, Facile Transferring of Wafer-Scale Ultrathin Alumina Membranes onto Substrates for Nanostructure Patterning, ACS Nano, 9 (2015) 8584-8591.
[26] Z.B. Zhan, F. Grote, Z.J. Wang, R. Xu, Y. Lei, Degenerating Plasmonic Modes to Enhance the Performance of Surface Plasmon Resonance for Application in Solar Energy Conversion, Adv. Energy Mater., 5 (2015) 201501654.
[27] Q. Fu, Z.B. Zhan, J.X. Dou, X.Z. Zheng, R. Xu, M.H. Wu, Y. Lei, Highly Reproducible and Sensitive SERS Substrates with Ag Inter-Nanoparticle Gaps of 5 nm Fabricated by Ultrathin Aluminum Mask Technique, ACS Appl. Mater. Interfaces, 7 (2015) 13322-13328.
[28] Z.B. Zhan, Y. Lei, Sub-100-nm Nanoparticle Arrays with Perfect Ordering and Tunable and Uniform Dimensions Fabricated by Combining Nanoimprinting with Ultrathin Alumina Membrane Technique, ACS Nano, 8 (2014) 3862-3868.
[29] Z.B. Zhan, R. Xu, Y. Mi, H.P. Zhao, Y. Lei, Highly Controllable Surface Plasmon Resonance Property by Heights of Ordered Nanoparticle Arrays Fabricated via a Non lithographic Route, ACS Nano, 9 (2015) 4583-4590.
[30] B. Abad, J. Maiz, M. Martin-Gonzalez, Rules to Determine Thermal Conductivity and Density of Anodic Aluminum Oxide (AAO) Membranes, J. Phys. Chem. C, 120 (2016) 5361-5370.
[31] I.T. Witting, T.C. Chasapis, F. Ricci, M. Peters, N.A. Heinz, G. Hautier, G.J. Snyder, Adv. Electron. Mater., 5 (2019) 1800904.
[32] O. Yamashita, S. Tomiyoshi, K. Makita, J. Appl. Phys., 93 (2003) 368-374.
[33] Z.B. Zhan, R. Xu, X.Z. Zheng, Q. Fu, M.H. Wu, Y. Lei, Effective approach to strengthen plasmon resonance localized on top surfaces of Ag nanoparticles and application in surface-enhanced Raman spectroscopy, Nanotechnology, 27 (2016) 445301.
[34] D.A. Borca-Tasciuc, G. Chen, Anisotropic thermal properties of nanochanneled alumina templates, J. Appl. Phys., 97 (2005) 084303.

Zhibing Zhan received his Ph.D degree in Materials Physics and Chemistry from Fujian Institute of Research on the Structure of Matter, Chinese Academy of Sciences. Currently, he is working as a postdoctoral researcher at the Institute of Optics, University of Rochester. His scientific research concentrates on femtosecond laser-matter interactions and functionalizing material surfaces through laser engineering: superhydrophilic and superhydrophobic surfaces; and novel micro/nano-hierarchical architectures by scalable laser-chemical hybrid method.

Dr. Mohamed ElKabbash did his bachelors in physics and economics from Illinois Wesleyan University, USA, and PhD in Physics from Case Western Reserve University, USA. His current research projects include ultrafast imaging of nanostructures, development of novel types of metasurfaces, developing hybrid solar energy based materials, and and developing novel thin-film metamaterials for optical switching, control of spontaneous emission rate, and enhanced third-order nonlinearity. Dr. Mohamed also has a bachelors and masters in Law and political economy from Alexandria University, Egypt.

 Zihao Li is a graduate student at the Institute of Optics, University of Rochester. His research interests mainly focus on surface microprocessing and optical properties of materials.

 Xiaoyun Li is an undergraduate student at the Institute of Optics, University of Rochester, majoring in Optics. He is working as an undergraduate research student in Professor Chunlei Guo's research group in University of Rochester. His research focuses primarily on the impact of laser imprinting on various surfaces withdifferent materials.

 Jihua Zhang is a postdoctoral associate in the Institute of Optics at University of Rochester. He obtained BS degree from Huazhong University of Science and Technology in 2011, and dual PhD degrees from University of Paris-Saclay and Huazhong University of Science and Technology in 2016. After that, he worked as a research associate in the Institute of Physics, Chinese Academy of Science for 6 months. His PhD research was focused on nonlinear integrated photonics. His current research interests are in metasurfaces and femtosecond laser nanofabrication.

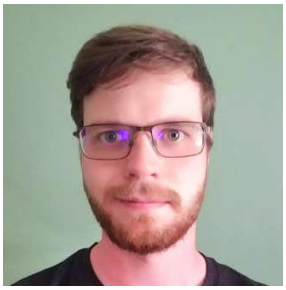

James Rutledge is a recent graduate from the University of Rochester with a degree in Optical Engineering. He worked as a technical assistant with the Guo lab to characterize nanomaterials along with numerous solar technologies.

S.C. Singh is currently Scientist at The Institute of Optics, University of Rochester, USA and Associate Professor at Guo's Photonics Laboratory, CIOMP, Changchun China. Hereceived his Ph.D. degree in 2009 from department ofPhysics, University of Allahabad, India. Dr. Singh has morethan eight years of research experience in the Physics andchemistry of materials and their applications in energyharvesting and storage. Dr. Singh served as main editor for Wiley-VCH book "Nanomaterials; Processing and char-acterization with lasers"and guest editor for special issuesof many journals.

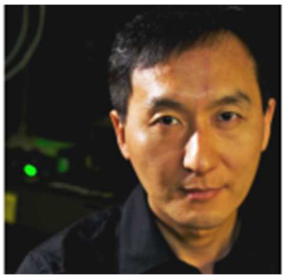

Chunlei Guo is a Professor in The Institute of Optics at University of Rochester. He also directs the Guo China-US Photonics Laboratory at CIOMP, China. His research is in the area of laser-matter interactions. His work at Rochester led to the discoveries of a range of highly functionalized materials, which may find a broad range of applications. He is a Fellow of American Physical Society and Optical Society of America. Currently, he serves as the Editor-in-Chief for CRC Handbook of Laser Technology and Applications (2nd Edition).

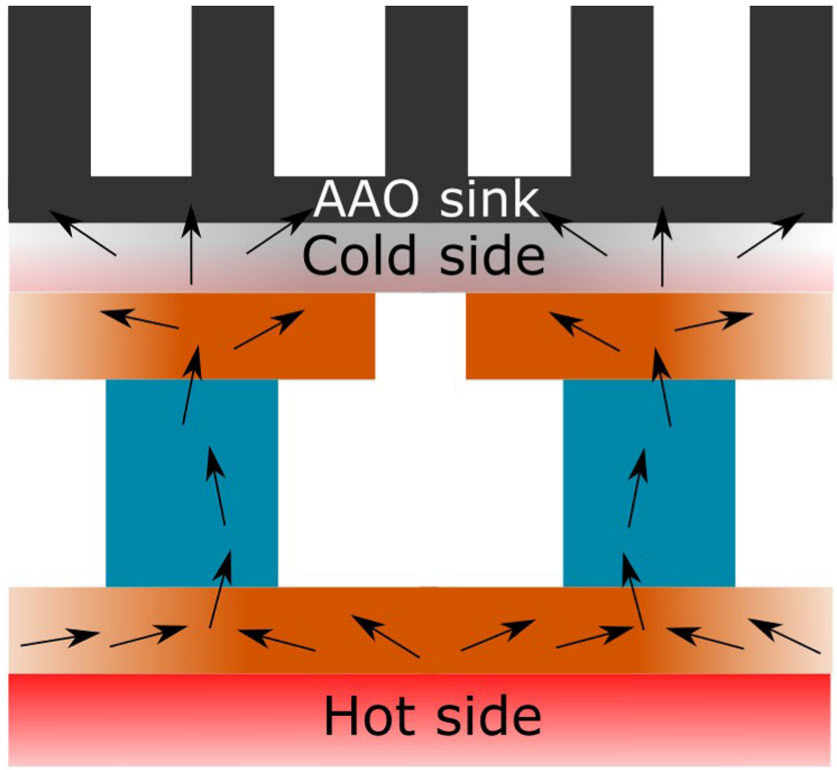
AAO sink
Cold side
Hot side

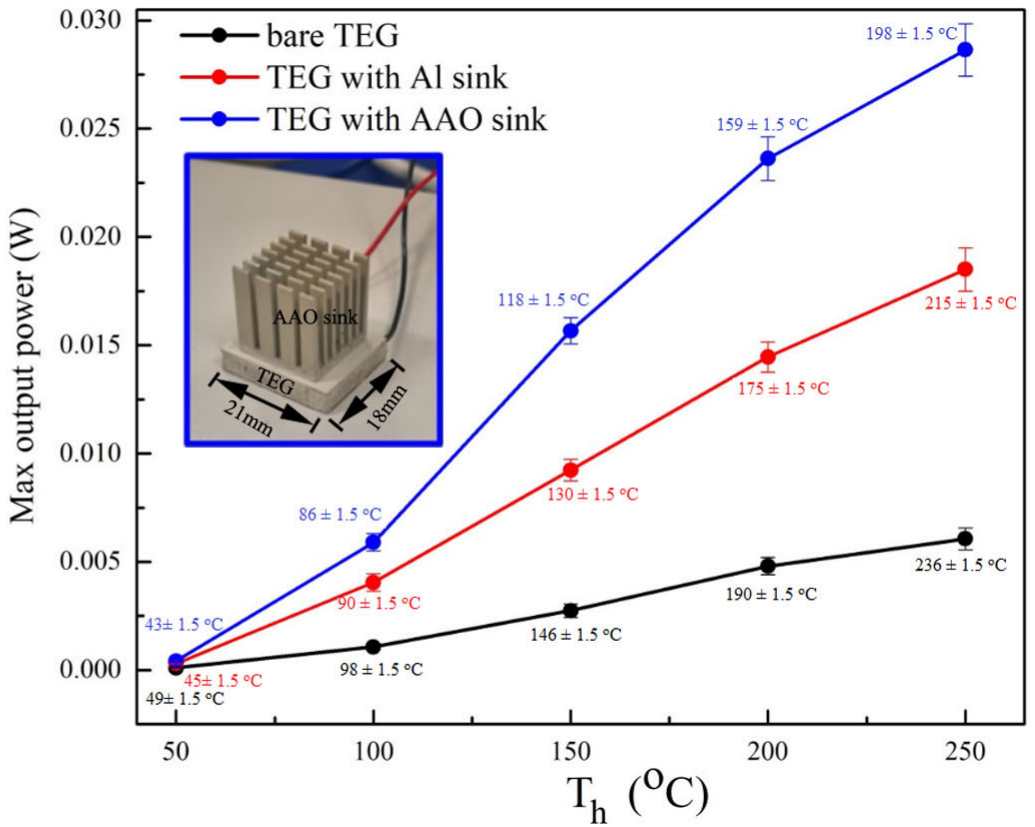
bare TEG
TEG with Al sink
TEG with AAO sink
Max output power (W)
0.030
0.025
0.020
0.015
0.010
0.005
0.000
50
100
150
200
250
T_h (°C)
AAO sink
TEG
21mm
18mm
198 ± 1.5 °C
159 ± 1.5 °C
118 ± 1.5 °C
86 ± 1.5 °C
43± 1.5 °C
215 ± 1.5 °C
175 ± 1.5 °C
130 ± 1.5 °C
90 ± 1.5 °C
45± 1.5 °C
236 ± 1.5 °C
190 ± 1.5 °C
146 ± 1.5 °C
98 ± 1.5 °C
49± 1.5 °C